FERMILAB-CONF-15-213-ND

RECENT RESULTS FROM MINERvA

C.E. PATRICK
Department of Physics and Astronomy, Northwestern University, 2145 Sheridan Road, Evanston, IL, 60208, USA

The MINERvA detector is situated in Fermilab's NuMI beam, which provides neutrinos and antineutrinos in the 1-20 GeV range. It is designed to make precision cross-section measurements for scattering processes on various nuclei. These proceedings summarize the differential cross-section distributions measured for several different processes. Comparison of these with various models hints at additional nuclear effects not included in common simulations. These results will help constrain generators' nuclear models and reduce systematic uncertainties on their predictions. An accurate cross-section model, with minimal uncertainties, is vital to oscillation experiments.

1 The MINERvA detector

MINERvA is situated in Fermilab's NuMI muon-neutrino beamline [1]. The results described in this talk were generated from data taken in the low-energy beam configuration between 2010 and 2012, with a peak neutrino energy around 3 GeV. During this period, we collected 3.98×10^{20} protons on target in the neutrino-enhanced configuration, and 1.7×10^{20} in the antineutrino. The detector is now taking data in a medium-energy configuration with a peak energy around 6 GeV.

The MINERvA detector's [2] central tracking region is constructed from 120 planes of parallel triangular strips of plastic (CH) scintillator, arranged almost perpendicular to the beam axis. Each strip contains a wavelength-shifting fiber, which delivers light generated by charged particles to photomultiplier tubes. Planes of these strips are oriented at (0, $\pm 60°$) to enable three-dimensional track reconstruction. Downstream and to the sides of the tracker are a lead electromagnetic calorimeter and a steel hadronic calorimeter, interspersed with scintillator. Upstream of the tracker, scintillator planes are interspersed with planes of nuclear target materials: iron, lead and graphite. A water target is also installed. Directly upstream of the detector is a liquid helium target. The magnetized MINOS [3] near detector, 2m downstream, acts as a muon spectrometer.

MINERvA's energy range of 1-20 GeV allows us to investigate three types [4] of neutrino-nucleon scattering. Quasi-elastic scattering, where a neutrino exchanges a W boson with a single

Operated by Fermi Research Alliance, LLC under Contract No. De-AC02-07CH11359 with the United States Department of Energy.

nucleon, is most prevalent at lower energies. Above 1GeV, we see significant contributions from resonant pion production. Deep inelastic scattering dominates above around 5 GeV.

2 Quasi-elastic scattering

2.1 Quasi-elastic scattering theory

Charged-current quasi-elastic (CCQE) interactions, $\nu_l n \rightarrow l^- p$ and $\bar{\nu}_l p \rightarrow l^+ n$, are important signal processes for oscillation experiments, and have been extensively studied due to their relative simplicity. When a neutrino scatters quasi-elastically from a stationary nucleon, it is possible to reconstruct the neutrino's energy, E_ν, and the four-momentum transfer, Q^2, from final-state lepton's kinematics. For neutrino scattering, Q^2 and E_ν can alternatively be calculated from the kinematics of the final-state proton. The differential cross-section $\frac{d\sigma}{dQ^2}$ can also be calculated [5] using the Llewellyn Smith formalism, as a function of Q^2 and various nucleon form-factors. All but one of these (the axial form-factor F_A) can be measured in electron scattering processes. With F_A modeled as a dipole, this leaves one free parameter, the axial mass, M_A, to be determined from neutrino scattering. Bubble chamber experiments on hydrogen and deuterium [7 11] give a global average value close to $M_A = 1.0 GeV/c^2$.

In heavy nuclei, however, nucleons are not stationary, and interact with each other; meaning that the Llewellyn Smith cross-section model must be modified to include these effects. The simplest model for this, the Relativistic Fermi Gas (RFG) [6] models the nucleons as independent particles, moving with a Fermi momentum distribution in a field generated by the rest of the nucleus. Additionally, the Pauli exclusion principle requires an ejected nucleon to have a momentum above the Fermi limit. The RFG, however, does not model additional nuclear effects due to nucleon-nucleon correlations [8]. Scattering from correlated pairs of nucleons can not only affect reconstruction, but can also lead to the additional ejection of the correlated partner. [12] Correlations can occur at short, medium, and long range, and can be generated in various ways.

Several models for some or all of these nuclear effects have been implemented. Our nominal Monte Carlo, GENIE 2.6.2 [17], includes the Bodek-Ritchie correction to the RFG [9 10], which models short-range correlations with a high-momentum tail. An alternative approach is to use a shell model of nuclear energy levels, modifying this spectral function [14] to include energies corresponding to correlated pairs. Amplitudes for Feynman diagrams corresponding to meson exchange currents (which lead to multi-nucleon effects, including correlations) have been calculated [13]. An enhancement found in electron-nucleon scattering, believed to be caused by correlation effects, can be modeled by a modification to the nucleon's magnetic form factor. This is known as the Transverse Enhancement Model [15].

In addition to these initial-state nuclear effects, we must also consider final-state interactions. Hadrons produced by neutrino scattering may re-interact as they propagate through the nucleus. This can affect not only the energy and angle of the final-state particles; it can also alter the number and type of particles in the final state. For example, a proton produced in quasi-elastic scattering may re-scatter and produce a pion; alternatively a pion produced in a resonant process may be absorbed, producing a quasi-elastic-like final state. These processes are particularly important when we rely on hadron kinematics for our reconstruction. GENIE models FSI with the INTRANUKE package [18].

2.2 Quasi-elastic cross-section, calculated from muon kinematics

MINERvA has calculated both the neutrino [21] and the antineutrino [20] differential cross section $\frac{d\sigma}{dQ^2_{QE}}$ in the scintillator tracker, where the four-momentum transfer, Q^2_{QE} and neutrino energy E_ν^{QE} are calculated from the kinematics of the final-state muon.

The MINOS near detector is used to identify correct-sign muons; the price of this is a limited acceptance as only forward going muons (less than 20° to the beam line, depending on

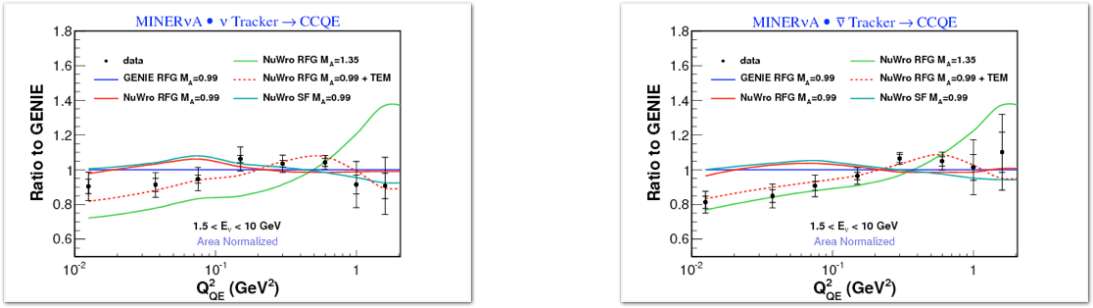

Figure 1 – Neutrino (left) and antineutrino (right) CCQE differential cross-section shapes in data and models, as a ratio to GENIE prediction. Muon kinematics have been used to reconstruct this sample.

the interaction's location) will hit MINOS.

In figure 1, we compare the shape of our measured cross-section distributions with various models. By looking at the shape, as opposed to absolute values, we can substantially reduce systematic uncertainties, particularly due to neutrino flux, which chiefly affects normalization. For clarity, we take a ratio to GENIE's [17] RFG model, with M_A of 0.99 GeV. We also compare to the NuWro [19] generator's RFG models with M_A of 0.99 GeV and 1.35 GeV (consistent with a lower-energy measurement from MiniBooNE [22]), as well as with its modeling of nuclear effects using spectral functions [14] and transverse enhancement (TEM) [15]. In both cases, the data agree most closely with the TEM, hinting at correlation effects.

2.3 Quasi-elastic cross-section, calculated from proton kinematics

In a complementary analysis [23], we reconstruct the event using the kinematics of a stopping proton (note that this requires an incoming neutrino; an antineutrino interaction would produce a neutron, which we cannot track). For this analysis, both a muon and at least one proton track must be identified; however, there is no requirement for the muon to be matched in MINOS. Proton tracks are distinguished from pions by a cut on energy deposition rate dE/dx; we also reject events with Michel electrons from the decay of a pion to a muon, which itself decays at rest. This analysis looks at events with a quasi-elastic-like signature (no pion tracks). In this case, we calculate Q^2 from the kinematics of the most energetic proton. The cross-section results are shown in figure 2. In contrast to figure 1 (which favored TEM), the closest agreement is to the unadorned RFG . However, there are several important differences between the two analyses. The lack of a MINOS match requirement means that the proton-kinematics study has a greater muon-angular acceptance; however, its low Q^2 range is restricted, due to the requirement for a trackable proton, with kinetic energy > 450 MeV. Additionally, FSI modeling becomes important, as the proton used to reconstruct the event may have re-interacted, changing its energy or angle.

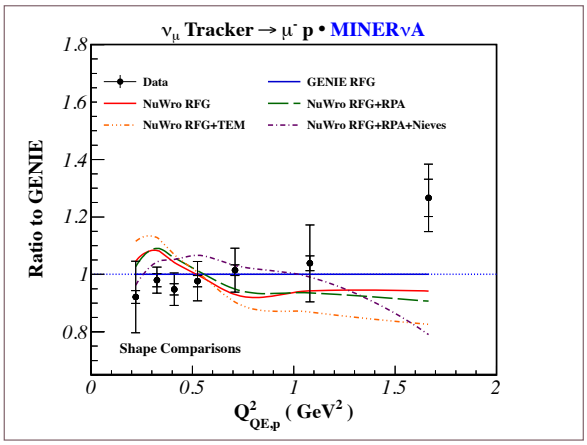

Figure 2 – Neutrino (left) quasi-elastic-like differential cross-section shape in data and models, as a ratio to GENIE. Proton kinematics have been used to reconstruct this sample.

This tension shows that we have not yet tested a theory which is able to accurately reproduce results across the whole phase space, regardless of how they are reconstructed. A complete nuclear quasi-elastic scattering theory should be able to reconcile with the data produced by

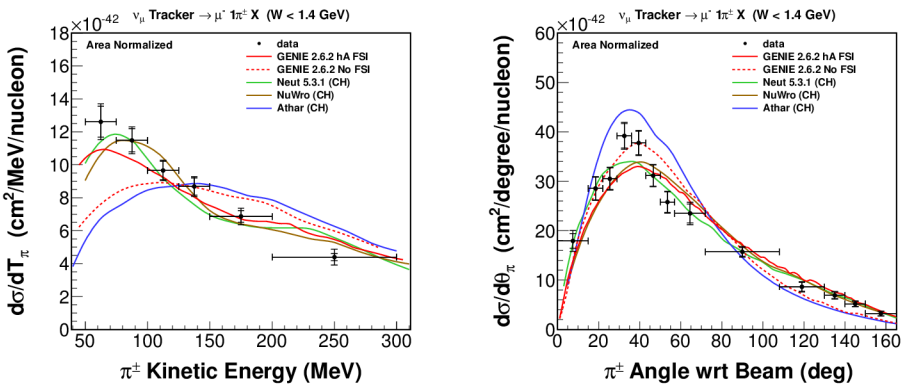

Figure 3 – Differential cross section vs. charged pion kinetic energy (left) and angle (right), in data and various models.

both methods. Further investigation of the quasi-elastic interaction is underway at MINERvA, and double-differential cross-sections (vs. muon parallel and transverse momentum) for both neutrino and antineutrino scattering on scintillator are currently being analyzed.

3 Pion production

3.1 Single charged-pion production form neutrino scattering

MINERvA has calculated the cross section for charged-current processes [27] in which a neutrino scatters from scintillator to produce a muon and a single charged pion ($\nu_\mu A \rightarrow \mu^- \pi^+ A$ or $\nu_\mu A \rightarrow \mu^- \pi^\pm X$ where A is the initial nucleus and X refers to the recoil nucleus (which may not be the same as A), plus any other particles that are not pions). The largest contribution to this comes from resonant processes, where the target nucleon is excited to a resonant state such as $\Delta(1232)$, which decays to a nucleon and pion. To select events with a single pion in the final state, a hadronic invariant mass $W < 1.4$ GeV is required.

Differential cross sections are measured with respect to the outgoing pion's kinetic energy and the angle between the pion and the neutrino beam. As before, we unfold our signal using GENIE [17], which models pion production using the Rein-Sehgal model [24]. We compare the results to GENIE,with and without final-state interactions enabled; to the models used in NuWro [19] and Neut [26], and to a model from Athar et al. [25], which does not include FSI.

The pion energy plot, in particular, shows the data's clear preference for models including FSI effects, highlighting the importance of these processes to pion energy distributions. The results of this study can be used by generators to constrain both the primary interaction rate for these processes and the FSI parameters.

3.2 Neutral pion production from antineutrino scattering

The cross section for charged-current neutral pion production from antineutrinos on scintillator ($\bar{\nu}_\mu A \rightarrow \mu^+ \pi^0 X$, where A and X are as in section 3.1), is not well-studied, and generators' models vary significantly. It is, however, important to oscillation experiments, as its neutral-current analog ($\bar{\nu}_\mu A \rightarrow \bar{\nu}_\mu \pi^0 X$) can mimic a $\bar{\nu}_e$ appearance signature, due to the electromagnetic shower of the $\pi^0 \rightarrow \gamma\gamma$ decay.

Figure 4 shows differential cross sections with respect to the kinetic energy and angle of the neutral pion. The pion is identified by looking for the two photon showers from its decay, and its energy and angle are reconstructed from the calorimetrically measured energy and the positions of these photons with respect to the muon vertex. The plots compare the measured cross section distributions to those predicted by GENIE [17] (with and without FSI), NuWro [19] and Neut [26], appearing to favor Neut's prediction. The generators differ in their FSI modeling methods; FSI

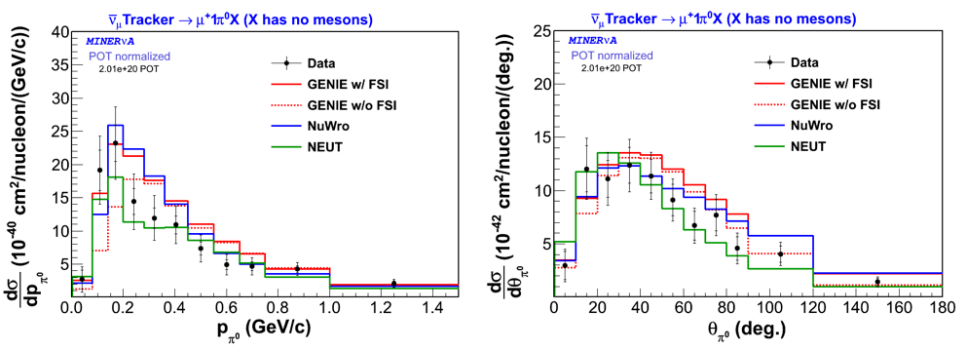

Figure 4 – Differential cross section vs. charged pion kinetic energy (left) and angle (right), in data and various models.

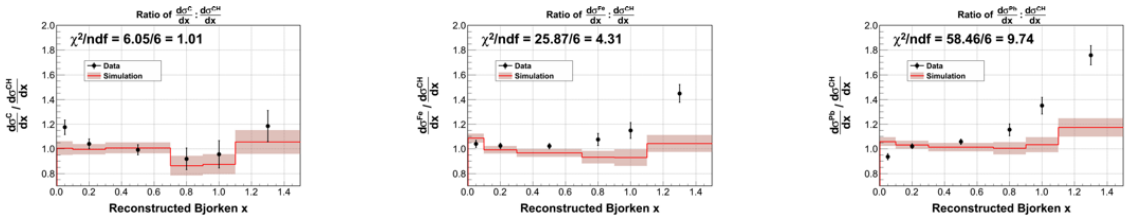

Figure 5 – Charged-current inclusive scattering differential cross section vs Bjorken x, as a ratio to CH scintillator, for increasingly heavy nuclei: carbon (left), iron (middle) and lead (right).

for pions is typically studied in pion beams, and as only charged pion beams are available, π^0 interaction rates must be inferred through isospin relations, leading to significant uncertainties. This measurement will be of use in evaluating the approximations made in generators' models.

4 Charged-current inclusive scattering from nuclear targets

The passive target region of the MINERvA detector allows us to compare scattering cross sections on different nuclei. A charged-current inclusive measurement [29] was made for neutrino scattering on graphite, iron, and lead targets, using events with a reconstructed $2 < E_\nu < 20$ GeV, ($\langle E_\nu \rangle = 8$ GeV). A MINOS-matched μ^- was required to identify charged-current neutrino scattering, limiting the sample to events with a muon angle below 17°.

Figure 5 shows the nucleus-to-scintillator ratio for the differential cross section, $\frac{d\sigma}{dx}$. Also shown is the GENIE [17] prediction. The x axis corresponds to the Bjorken scaling variable $x = \frac{Q^2}{2m\nu}$, which characterizes the type of interaction. Low x corresponds to the region where nuclear shadowing predicts a decreased cross section for heavier nuclei; our data show GENIE is under-predicting this effect. At high x, corresponding mainly to quasi-elastic interactions, GENIE under-predicts the cross section increasingly for heavier nuclei. This may be because GENIE does not include meson-exchange current interactions. In both cases, further study is needed to investigate these effects, and the increased statistics of MINERvA's medium-energy run should provide ample data for further analysis of elastic and deep inelastic scattering distributions in the nuclear targets.

Acknowledgments

This work was supported by the Fermi National Accelerator Laboratory under US Department of Energy contract No. DEAC02-07CH11359 which included the MINERvA construction project. Construction support also was granted by the United States National Science Foundation under Award PHY-0619727 and by the University of Rochester. Support for participating scientists was provided by NSF and DOE (USA) by CAPES and CNPq (Brazil), by CoNaCyT (Mexico), by

CONICYT (Chile), by CONCYTEC, DGI-PUCP and IDI/IGI-UNI (Peru), by Latin American Center for Physics (CLAF), by the Swiss National Science Foundation, and by RAS and the Russian Ministry of Education and Science (Russia). We thank the MINOS Collaboration for use of its near detector data. Finally, we thank the staff of Fermilab for support of the beamline and the detector.

References

1. K. Anderson, B. Bernstein, D. Boehnlein, K. R. Bourkland, S. Childress, et al.,FERMILAB-DESIGN **1998**, 01 (1998)
2. L. Aliaga et al. (The MINERvA Collaboration) *Nucl. Instrum. Methods* **A743**, 130 (2014)
3. D.G. Michael et al. (MINOS Collaboration), *Nucl. Instrum. Methods* **A596**, 190 (2008)
4. J.A. Formaggio and G.P. Zeller, *Rev. Mod. Phys.* **84**, 1307-1341 (2012)
5. C.H. Llewellyn Smith, *Phys. Rept.* **3C**, 261 (1972).
6. R. Smith and E. Moniz, *Nucl. Phys.* B **43**, 605 (1972).
7. A. Bodek, S. Avvakumov, R. Bradford, and H. S. Budd, *J.Phys.Conf.Ser.* **110**, 082004 (2008).
8. O. Lalakulich, U. Mosel, and K. Gallmeister *Phys. Rev. C* **86**, 054606 (2012)
9. A. Bodek, and J. L. Ritchie, *Phys. Rev.* D **23**, 1070 (1980).
10. A. Bodek, and J. L. Ritchie, *Phys. Rev.* D **24**, 1400 (1981).
11. AK. S. Kuzmin, V. V. Lyubushkin, and V. A. Naumov, *Eur. Phys. J.* **C54**, 517 (2008).
12. R. Subedi et al., *Science* **320**, 1476 (2008).
13. J. Nieves, I. Ruiz Simo and M. J. Vicente Vacas, *Phys. Rev. C* **83**, 045501 (2011).
14. O. Benhar, A. Fabrocini, S. Fantoni, and I. Sick, *Nucl.Phys. A* **579**, 493 (1994).
15. A. Bodek, H. Budd, and M. Christy, *Eur. Phys. J.* **C71**, 1726 (2011).
16. J. Carlson et al, *Phys. Rev. C* **65**, 024002 (2002).
17. C. Andreopoulos, et al., *Nucl. Instrum. Methods* **288A**, 87 (2010).
18. S. Dytman, *AIP Conf Proc* **896**, 178-184 (2007)
19. K. M. Graczyk and J. T. Sobczyk, *Eur. Phys. J.* **C31**, 177 (2003).
20. L. Fields, J. Chvojka et al. (The MINERvA Collaboration), *Phys. Rev. Lett.* **111**, 022501 (2013).
21. G.A. Fiorentini, D. Schmitz et al. (The MINERvA Collaboration), *Phys. Rev. Lett.* **111**, 022502 (2013).
22. A. A. Aguilar-Arevalo et al. (MiniBooNE Collaboration), *Phys. Rev. Lett.* **100**, 032301 (2008)
23. T. Walton, M. Betancourt et al. (The MINERvA Collaboration), *Phys. Rev.* D **91**, 071301 (2015).
24. D. Rein and L. M. Sehgal, *Ann. Phys.* **133**, 79 (1981)
25. Athar, M., Chauhan, S., and Singh, S. K., *Eur. Phys. J.* **A43**, 209-227 (2010).
26. Y. Hayato, *Acta Phys.Polon.* **B40**, 2477-2489 (2009).
27. B. Eberly et al. (The MINERvA Collaboration), arXiv:1406.6415 [hep-ex]
28. T. Le et al. (The MINERvA Collaboration), arXiv:1503.02107 [hep-ex]
29. B. Tice et al, (The MINERvA Collaboration), PRL **112**, 231801 (2014)